Physics of Fluids

On Stokes' second problem solutions in cylindrical and Cartesian domains

Cite as: Phys. Fluids **34**, 103615 (2022); https://doi.org/10.1063/5.0118838
Submitted: 06 August 2022 • Accepted: 26 September 2022 • Accepted Manuscript Online: 27 September 2022 • Published Online: 27 October 2022

Daniel J. Coxe, Yulia T. Peet and Ronald J. Adrian

Physics of Fluids ARTICLE scitation.org/journal/phf

On Stokes' second problem solutions in cylindrical and Cartesian domains

Cite as: Phys. Fluids **34**, 103615 (2022); doi: 10.1063/5.0118838
Submitted: 6 August 2022 · Accepted: 26 September 2022 ·
Published Online: 27 October 2022

Daniel J. Coxe,[a] Yulia T. Peet,[b] and Ronald J. Adrian[c]

AFFILIATIONS

School for Engineering of Matter Transport and Energy, Arizona State University, Tempe, Arizona 85287, USA

[a]Author to whom correspondence should be addressed: dcoxe@asu.edu
[b]Electronic mail: ypeet@asu.edu
[c]Electronic mail: rjadrian@asu.edu

ABSTRACT

It is well known that drag created by turbulent flow over a surface can be reduced by oscillating the surface in the direction transverse to the mean flow. Efforts to understand the mechanism by which this occurs often apply the solution for laminar flow in the infinite half-space over a planar, oscillating wall (Stokes' second problem) through the viscous and buffer layer of the streamwise turbulent flow. This approach is used for flows having planar surfaces, such as channel flow, and flows over curved surfaces, such as the interior of round pipes. However, surface curvature introduces an additional effect that can be significant, especially when the viscous region is not small compared to the pipe radius. The exact solutions for flow over transversely oscillating walls in a laminar pipe and planar channel flow are compared to the solution of Stokes' second problem to determine the effects of wall curvature and/or finite domain size. It is shown that a single non-dimensional parameter, the Womersley number, can be used to scale these effects and that both effects become small at a Womersley number of greater than about 6.51, which is the Womersley number based on the thickness of the Stokes' layer of the classical solution.

NOMENCLATURE

Symbol

h	Channel half height (m)
r	Radial coordinate (m)
R	Pipe radius (m)
Re_τ	Reynolds number (49)
t	Time (s)
T	Non-dimensional time (6)
u_θ	Azimuthal velocity component (m/s)
u_τ	Wall friction velocity
w	Spanwise velocity component (m/s)
w_0	Wall velocity amplitude (m/s), (5) and (20)
$W\text{cyl}$	Non-dimensional azimuthal velocity (19)
W_1	Non-dimensional spanwise velocity of HOW (11)
W_2	Non-dimensional wall velocity of the APW (15)
y	Wall normal coordinate (m)
α	Stokes' depth (m) (8)
ξ	Non-dimensional wall normal coordinate (26), (28), and (30)
ν	Kinematic viscosity (m^2/s)
ρ	Fluid density (kg/m^3)
ω	Frequency of wall oscillation (rad/s)
$\mathcal{W}_o$	Womersely number (14)

I. INTRODUCTION

Oscillation of a plane wall transverse to a direction of turbulent flow is known to reduce drag.[1,2] Drag reduction up to 40% has been reported from experiments[3] and 35% from DNS.[4] In laminar flows, transverse wall oscillation creates a Stokes' layer of positive and negative transverse velocities[5,6] whose extent above the wall depends on the square root of kinematic viscosity and frequency of wall oscillation. In the wall bounded turbulent shear flow, in the x direction, the z-ward transverse wall oscillation is thought to reduce drag most effectively when the frequency is tuned to place the Stokes' layer within the buffer layer.[7,8] Although the Stokes' layer unquestionably influences the creation of turbulence near the wall, there is a disagreement over the physics of the process. Touber and Leschziner[9] argue the Stokes' layer increases the size of the viscous sublayer and diminishes ejections and sweeps. The Stokes' layer is hypothesized to interact with the quasi-streamwise vortices located in the buffer layer of the flow in such a

way that it weakens these turbulent events known to be associated with a drag increase. Ricco and Quadrio[10] argue that the wall oscillations increase the buffer layer thickness. They also provide an empirical model for a drag reduction estimation depending on the wall oscillation parameters in channel flows.[10] Unarguably, investigating the physics of turbulence modification by spanwise wall oscillation continues to be a topic of interest. Since drag reduction in pipes was observed to be greater than that of boundary layers or channels, we ask what makes the Stokes' layer in pipes different from that of plane walls.

To answer this question, we have considered three problems of laminar viscous flows: (a) Stokes' second problem,[5] the classic solution for flow in the half-space overlying a plane that is oscillating with transverse wall velocity $w|_{\text{wall}} = w_0 \sin(\omega t)$ referred to as the half-space oscillating wall (HOW), (b) laminar viscous flow in a space bounded by two infinite plane walls that oscillate 180° out of phase, referred to as anti-phase parallel walls (APW), and (c) flow in a cylindrical pipe wall that oscillates with velocity $u_\theta|_{\text{wall}} = w_0 \sin(\omega t)$ (OPW).[11] The geometry of the pipe differs fundamentally from Stokes' planar flow (HOW) in two ways: the pipe domain is bounded and its boundary is curved. To eliminate the effect of unbounded domain, the second case was devised. The two-plane wall case (APW) is analogous to Stokes' second problem, but its velocity must be anti-symmetric about the centerline. Qualitatively, the Stokes' layer in (a), (b), and (c) are similar.

The Stokes' layer concept has been employed by many investigators to understand how transverse oscillatory motion of the wall modifies turbulence and accomplishes drag reduction.[12,13] Different types of transverse wall motions have also been studied in other contexts[14–19] to understand the effect of problem parameters on a near wall layer solution. However, the emphasis of this paper will be on Stokes' second problem on a half space and how it is modified by problem geometry. A laminar Stokes' second problem solution was shown by Ricco and Quadrio[10] to be a good approximation to a phase-averaged spanwise velocity profile in a turbulent flow above oscillated walls in a regime of drag reduction. While Stokes' second problem has been extended to more complicated geometries, including flow between one oscillating and one stationary plate,[20] flow in a half-channel above an oscillating plate with a stress-free (Neumann) condition at the top boundary,[21,22] and two-dimensional problems involving touching semi-infinite plates, one oscillating and one stationary, in both infinite[21–23] and finite[22] wall normal domains. Additionally, Song and Rau[11] recently explained the solution for Stokes' second problem in cylindrical geometry. While the derivation of solutions is not the focus of the current paper, and we are more interested in analysis of their differences, a solution between two plates oscillating out of phase does not seem to be available in the previous literature, so we present its derivation. Additionally, Song and Rau's[11] solution is complicated by the inclusion of the effects of initial transients, and, for our purposes, we are interested in fully developed time periodic flows; thus, we present an alternative solution of a cylindrical problem following the steps similar to the ones used in a derivation of the classical Stokes' second problem using separation of variables.[5]

The paper is organized as follows. In Sec. III, we present the solutions and, whenever applicable, their derivations for the three introduced Stokes' problems; in Sec. IV, we analyze the errors and discuss the influence of a finite size domain and a curvature on the solution differences; and in Sec. V, we draw conclusions.

II. SOLUTIONS TO STOKES' SECOND PROBLEM AND MODIFIED STOKES' PROBLEMS

A. Half-space oscillating wall

In Cartesian coordinates, the incompressible Navier–Stokes equations are given by the momentum and continuity equations as follows:

$$\frac{D}{Dt}\vec{u} = -\nabla p + \nu\nabla^2\vec{u}, \tag{1}$$

$$\nabla \cdot \vec{u} = 0. \tag{2}$$

The velocity is given by $\vec{u} = u\hat{i} + v\hat{j} + w\hat{k}$, where $\hat{i}, \hat{j}$, and $\hat{k}$ are the unit vectors in the x, y, and z coordinates, respectively, p corresponds to the pressure, and ν represents the kinematic viscosity. Furthermore, D/Dt denotes a material derivative, ∇ is the gradient operator $\nabla = \frac{\partial}{\partial x}\hat{i} + \frac{\partial}{\partial y}\hat{j} + \frac{\partial}{\partial z}\hat{k}$, and ∇^2 is the Laplacian operator $\nabla^2 = \frac{\partial^2}{\partial x^2} + \frac{\partial^2}{\partial y^2} + \frac{\partial^2}{\partial z^2}$.

Classical Stokes' second problem considers an infinite plate in the y–z plane located at $y = 0$ under an infinite boundary of the fluid. The wall oscillates in a spanwise (z) direction with a velocity $w_0 \sin(\omega t)$, where ω is the frequency of the oscillations. Under these assumptions, the governing equations of motion (1) and (2) in a laminar flow reduce to

$$\frac{\partial w}{\partial t} - \nu\frac{\partial^2 w}{\partial y^2} = 0. \tag{3}$$

The boundary conditions are specified as $w(y = 0, t) = w_0 \sin(\omega t)$, $w(y \to \infty, t) = 0$. Using the wall velocity amplitude w_0, oscillation frequency ω, and viscosity ν as the reference dimensional parameters, a non-dimensional equation can be formed as

$$\frac{\partial W}{\partial T} - \frac{\partial^2 W}{\partial Y^2} = 0, \tag{4}$$

$$W = \frac{w}{w_0}, \tag{5}$$

$$T = \omega t, \tag{6}$$

$$Y = \frac{y}{\alpha}, \tag{7}$$

$$\alpha = \sqrt{\frac{\nu}{\omega}}, \tag{8}$$

with boundary conditions

$$W(Y = 0, T) = \sin(T), \tag{9}$$

$$W(Y \to \infty, T) = 0. \tag{10}$$

The solution of (4) with (9) and (10) is[5]

$$W_1(Y, T) = \Im\left\{\exp(iT)\exp\left(-\sqrt{i}Y\right)\right\}, \tag{11}$$

where $i = \sqrt{-1}$, and $\Im$ indicates the imaginary part of the solution.

B. Anti-phase parallel walls

The APW problem is formulated as follows. Two infinitely long parallel plates are located at $y = -h$ and $y = h$ and are oscillated out of phase, with velocities $w|_{y=-h} = w_0 \sin(\omega, t)$,

$w|_{y=h} = -w_0 \sin(\omega, t)$, respectively. Using the adopted normalization of Eqs. (5)–(8), (4), as previously, describes the governing equation of motion for the fluid between the plates, while the boundary conditions are given by

$$W(Y = -\mathcal{W}_o, T) = \sin(T), \tag{12}$$

$$W(Y = \mathcal{W}_o, T) = -\sin(T). \tag{13}$$

For a finite-size domain, we have introduced the parameter $\mathcal{W}_o$, denoted as the Stokes' second problem Womersley number

$$\mathcal{W}_o = h/\alpha = h\sqrt{\frac{\omega}{\nu}}. \tag{14}$$

The solution to Eq. (4) with the boundary conditions (12) and (13) can be written as follows, and the solution process can be found in Appendix A,

$$W_2(Y, T) = \Im\left\{-\exp(iT)\frac{\sinh\left(\sqrt{i}Y\right)}{\sinh\left(\sqrt{i}\mathcal{W}o\right)}\right\}. \tag{15}$$

This solution returns a zero velocity at the centerline, $Y = 0$, as expected.

C. Oscillating pipe wall

The incompressible Navier–Stokes equations in the cylindrical coordinates are given by

$$\frac{\partial u_x}{\partial t} + u_r\frac{\partial u_x}{\partial r} + \frac{u_\theta}{r}\frac{\partial u_x}{\partial \theta} + u_x\frac{\partial u_x}{\partial x} = -\frac{\partial p}{\partial x} + \nu\nabla^2 u_x, \tag{16}$$

$$\frac{\partial u_r}{\partial t} + u_r\frac{\partial u_r}{\partial r} + \frac{u_\theta}{r}\frac{\partial u_r}{\partial \theta} + u_x\frac{\partial u_x}{\partial x} - \frac{u_\theta^2}{r} = -\frac{\partial p}{\partial r} + \nu\nabla^2 u_r, \tag{17}$$

$$\frac{\partial u_\theta}{\partial t} + u_r\frac{\partial u_\theta}{\partial r} + \frac{u_\theta}{r}\frac{\partial u_\theta}{\partial \theta} + u_x\frac{\partial u_\theta}{\partial x} + \frac{u_\theta u_r}{r} = -\frac{1}{r}\frac{\partial p}{\partial \theta} + \nu\nabla^2 u_\theta, \tag{18}$$

where $\{r, \theta, x\}$ correspond to a radial, azimuthal, and longitudinal directions, respectively, and $\{u_r, u_\theta, u_x\}$ denote the corresponding velocity components. In the context of cylindrical coordinates, the Laplacian operator, ∇^2 is given as $\nabla^2 = \frac{1}{r}\frac{\partial}{\partial r}\left(r\frac{\partial}{\partial r}\right) + \frac{1}{r^2}\frac{\partial}{\partial \theta^2} + \frac{\partial^2}{\partial x^2}$.

For the Stokes' second problem in the cylindrical coordinates, the fluid domain is inside a round pipe of a diameter D, and a pipe wall oscillates with velocity $w_0 \sin(\omega t)$ in an azimuthal direction. Under these assumptions, we can set $u_r = u_x = 0$ and $\partial u_\theta/\partial\theta = 0$.

The solution to the Stokes' second problem in cylindrical coordinates using Laplace transform that considers initial transients can be found in the work of Song and Rau.[11] However, in the current work, we are primarily interested in fully developed time-periodic solutions because these solutions are most representative of the data acquired by researchers investigating drag reduction in fully developed pipe flows with wall oscillations.[3,24,25] An alternative derivation directly geared to finding a time-periodic solution is presented in Appendix B, and such solution is given as

$$W_{cyl}(R, T) = \Im\left\{\exp(iT)\frac{J_1\left(\sqrt{i^3}R\right)}{J_1\left(\sqrt{i^3}\mathcal{W}o\right)}\right\}, \tag{19}$$

where the non-dimensional variables are defined as

$$W = \frac{u_\theta}{w_0}, \tag{20}$$

$$T = \omega t, \tag{21}$$

$$R = \frac{r}{\alpha}, \tag{22}$$

$$\mathcal{W}_o = \frac{D}{2\alpha}, \tag{23}$$

$$\alpha = \sqrt{\frac{\nu}{\omega}}, \tag{24}$$

and J_1 is the Bessel function of the first kind.

III. COMPARISON OF SOLUTIONS

A. Domain choice and rescaling of solutions

The objective of this paper is to characterize how well the two Stokes' second problem solutions based on Cartesian geometries (HOW and APW) approximate a solution to the Stokes' second problem in cylindrical coordinates (OPW). However, while doing so, we face a problem that the two finite-domain solutions (OPW and AOW) have a clearly defined length scale related to the finite domain size, manifesting itself, in its normalized form, through the Womersley number defined in Eqs. (14) and (23). However, the classical Stokes' second problem defined in the infinite half-space, HOW, does not have this length scale. In order to compare finite domain solutions with an infinite domain solution, we need to artificially introduce such a length scale into the HOW problem, which, effectively, will truncate the comparison domain for the HOW solution. For comparison with finite domain solutions, we choose to define this length scale to be based on the sizes of the finite domains, which are h for the APW and $D/2$ for the OPW, matched through the selection of the Womerseley number $\mathcal{W}_o = h/\alpha = D/(2\alpha)$. We, therefore, define the domain size for the infinite half-space problem as $\delta = \mathcal{W}_o\,\alpha$, so that all three solutions are mapped to the same domain $\xi \in [0, \mathcal{W}_o]$ in the normalized wall-normal coordinate ξ, where ξ represents the normalized distance from the wall defined below for the three problems of interest.

HOW. For the HOW solution, $\xi = Y$, and the infinite-domain HOW solution of Eq. (11) mapped into the finite domain takes the following form:

$$W_1(\xi, T) = \Im\left\{\exp(iT)\exp\left(-\sqrt{i}\xi\right)\right\}, \tag{25}$$

$$0 \le \xi \le \frac{\delta}{\alpha}, \quad \delta = \mathcal{W}_o\,\alpha. \tag{26}$$

APW. For the APW, we define $\xi = Y - \mathcal{W}_o$, and the solution (15) is written as

$$W_2(\xi, T) = \Im\left\{\exp(iT)\frac{\sinh\left(\sqrt{i}(\mathcal{W}_o - \xi)\right)}{\sinh\left(\sqrt{i}\mathcal{W}_o\right)}\right\}, \tag{27}$$

$$0 \le \xi \le \frac{h}{\alpha}. \tag{28}$$

OPW. To define a normalized distance from the wall for the pipe geometry, we set $\xi = \mathcal{W}_o - R$, which transforms Eq. (19) into

$$W_{cyl}(\xi, T) = \Im\left\{\exp(iT)\frac{J_1(\sqrt{i^3}(\mathcal{W}_o - \xi))}{J_1\left(\sqrt{i^3}\mathcal{W}_o\right)}\right\}, \tag{29}$$

$$0 \le \xi \le \frac{D}{2\alpha}. \tag{30}$$

To further illustrate the effect of the HOW domain truncation on the solution comparison, we plot in Fig. 1 the normalized distance to the wall-normal location where the velocity in the Stokes' layer decays to 1% of its value at the wall for the three problems, defined as

$$\xi^{1\%} = \xi : W_i(\xi, T = \pi/2) = 0.01, \tag{31}$$

where $i = 1, 2, cyl$, corresponding to HOW, APW, and OPW solutions, respectively. For the HOW problem, such distance is independent of the Womersely number and is equal to the normalized Stokes' layer thickness, where Stokes' layer thickness, δ^{Sl}, can be computed from the analytical solution (11) to the standard Stokes' second problem as[5]

$$\delta^{Sl} = 4.6\sqrt{2\nu/\omega} = 4.6\sqrt{2}\,\alpha. \tag{32}$$

We note that the Stokes' layer thickness in Eq. (32) is different from the Stokes' penetration depth $\delta^{Sp} = \sqrt{2\,\nu/\omega}$ commonly used in the definition of the Stokes' problem,[26,27] with the relationship

$$\delta^{Sl} = 4.6\,\delta^{Sp}. \tag{33}$$

We can further define a Womersley number based on Stokes' layer thickness as

$$\mathcal{W}_o^{Sl} = \delta^{Sl}\sqrt{\frac{\omega}{\nu}} = 4.6\sqrt{2} \approx 6.51. \tag{34}$$

For the APW and OPW problems, $\xi^{1\%}$ roughly scales with the domain size for Womersley numbers $\mathcal{W}_o \lesssim \mathcal{W}_o^{Sl}$, since in these cases the distance to the center of the domain, where velocity drops to zero due to geometrical constraints, is smaller than the corresponding distance δ^{Sl} imposed by the nature of the Stokes' solution. After $\mathcal{W}_o$ reaches $\mathcal{W}_o^{Sl}$, this distance is unchanged for the three problems and is equivalent to δ^{Sl}, as seen from Fig. 1. Therefore, truncating the HOW domain to $\delta = \mathcal{W}_o\,\alpha$ leads to the fact that, for low Womersley numbers, the velocity value for the HOW solution at the top domain boundary would be higher than 1% of the wall velocity, while it drops to zero in the corresponding APW and OPW domains, contributing to the solution mismatch as discussed in the next section. This is a consequence of the comparison of solutions in unbounded and finite-size domains.

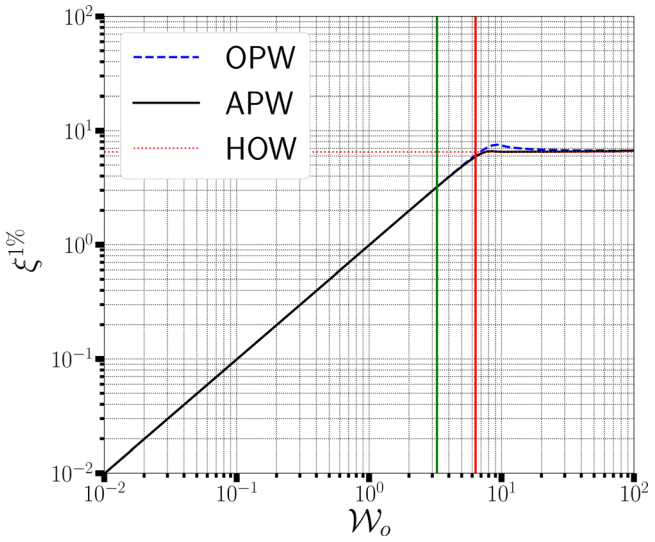

FIG. 1. Normalized distance to the wall-normal location, where the velocity in the Stokes' layer decays to 1% of its wall value for the three problems, $\xi^{1\%}$, vs $\mathcal{W}_o$ number. For the HOW problem, such distance is independent of $\mathcal{W}_o$ and equals to the Stokes' layer thickness $\delta^{Sl}/\alpha = 4.6\sqrt{2} \approx 6.51$. For the APW and OPW problems, this distance first increases with the domain size (or $\mathcal{W}_o$) until it reaches δ^{Sl}/α. The green vertical line indicates a $\mathcal{W}_o = 3.26$ where the error between OPW and APW is maximized (Fig. 2), while the red vertical line indicates the location of $\mathcal{W}_o = 4.6\sqrt{2}$.

B. Error definition

To define the error, we consider cylindrical solution (OPW) as the baseline solution, from which the errors are calculated as

$$e_i(\xi, T) = W_i(\xi, T) - W_{cyl}(\xi, T), \tag{35}$$

for $i = 1$, 2, where $i = 1$ corresponds to a standard Stokes' problem solution (HOW) given by Eq. (25) and $i = 2$ corresponds to a finite domain Cartesian solution (APW) given by Eq. (27).

Since the errors are both space- and time-dependent, we define the L_2 error as

$$e_i^{L_2}(\mathcal{W}_o) = \left(\frac{1}{\mathcal{W}_o}\int_0^{\mathcal{W}_o}\frac{1}{2\pi}\int_0^{2\pi} e_i^2(\xi, T)\,dT\,d\xi\right)^{1/2}. \tag{36}$$

Due to a complexity of an analytical integration of the squared error profiles, the integral in Eq. (36) is evaluated numerically using $N = 64$ equidistant points in time and $M = 256$ Gauss–Legendre–Lobatto quadrature points[28] in space.

C. Dependence of error on Womersley number

Figure 2 shows the error profiles as a function of the Womersley number. As expected, for low Womersley number, the error between the standard Stokes' second problem (HOW) solution and the cylindrical (OPW) solution is large; however, it decreases with the increase in Womersley number. Unexpectedly, we observe that the error between the two-plate solution (APW) and the cylindrical solution (OPW) agrees well at low Womersley number, then increases to a maximum at $\mathcal{W}_o \approx 3.26$. For higher $\mathcal{W}_o$, the two error profiles collapse. It is worth noting that the error between the cylindrical solution and the finite-domain two-plate solution is always smaller than the error between the cylindrical and the infinite domain Stokes' solution, as expected.

D. Errors and velocity profiles at different flow regimes

We now examine the behavior of errors and velocity profiles at different flow regimes, in order to further understand the reasons contributing to the differences between the solutions.

Based on Fig. 2, we can identify three distinct flow regimes: (1) low Womersley number, $\mathcal{W}_0 \lesssim 0.1$; (2) intermediate Womersley number, $0.1 \lesssim \mathcal{W}_o \lesssim \mathcal{W}_o^{Sl}$ (the e_2 error exhibits a maximum in this regime at $\mathcal{W}_o \approx 3.26$); and (3) high Womersley number, $\mathcal{W}_o \gtrsim \mathcal{W}_o^{Sl}$. We will investigate each of these three flow regimes carefully in this

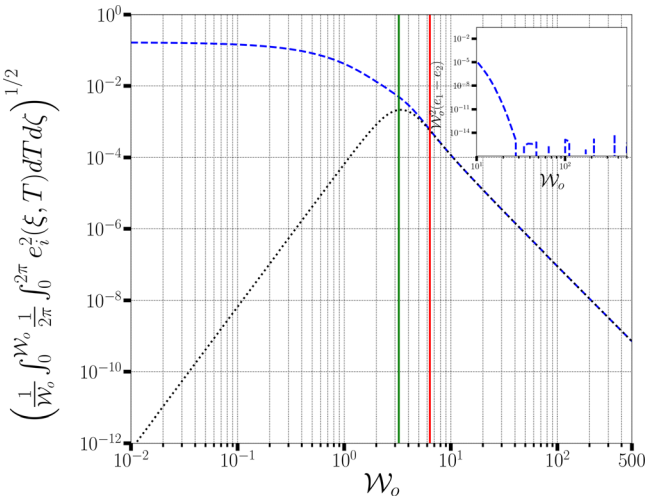

FIG. 2. L_2 error values vs Womersley number. Blues dashed line is e_1 comparing OPW and HOW solutions, and black dotted line is e_2 comparing OPW and APW solutions. The green vertical line indicates a $\mathcal{W}_o = 3.26$ where the error between OPW and APW is maximized, while the red vertical line indicates the location of $\mathcal{W}_o = 4.6\sqrt{2}$. The inset shows the difference between e_1 and e_2 multiplied by the square of $\mathcal{W}_o$.

section. Note that for low and high Womersley numbers, an asymptotic expansion of the solutions can be utilized to explain the error behavior, but not for the intermediate $\mathcal{W}_o$ regime.

To examine the dependence of the errors on a spatial location within the flow, in this section, we will look at a temporally averaged but spatially varying L_2 error defined as

$$e_i^{L_2}(\mathcal{W}_o, \xi) = \frac{1}{2\pi}\int_0^{2\pi} e_i^2(\xi, T)dT. \tag{37}$$

1. Low Womersley number flow

The velocity profiles for a low Womersley number flow are illustrated in Fig. 3 for $\mathcal{W}_o = 0.01$. To understand the behavior of errors and velocity profiles at a low Womersley number, we consider an asymptotic expansion of the three solutions at a limit $\mathcal{W}_o \to 0$.

HOW. For the standard Stokes' second problem, a Taylor expansion of the Eq. (25) for the region near the wall takes the following form:

$$W_1(\xi, T) \sim \Im\left\{\exp(iT)\left(1 - \sqrt{i}\xi\right)\right\}, \quad \xi \to 0. \tag{38}$$

Note the absence of the Womersley number in this expansion.

APW. For the APW solution (27), a Taylor series expansion of a hyperbolic sine function can be used to derive a low $\mathcal{W}_o$ approximation as

$$W_2(\xi, T) \sim \Im\left\{\exp(iT)\frac{\mathcal{W}_o - \xi}{\mathcal{W}_o}\right\}, \quad \mathcal{W}_o \to 0, \xi \to 0. \tag{39}$$

OPW. For a small value of its argument, there exists an asymptotic approximation for a Bessel function of the first kind shown by Abramowitz and Stegun[29]

$$J_1(z) \sim \frac{z}{2}, z \to 0. \tag{40}$$

Since the argument of the Bessel function in the OPW solution given by Eq. (29), $z = \sqrt{i^3}(\mathcal{W}_o - \xi)$, varies between 0 and $\sqrt{i^3}\mathcal{W}_o$, then, for sufficiently small Womersley numbers, the asymptotic form of the solution to a cylindrical Stokes' problem is obtained as

$$W_{\text{cyl}}(\xi, T) \sim \Im\left\{\exp(iT)\frac{\mathcal{W}_o - \xi}{\mathcal{W}_o}\right\}, \quad \mathcal{W}_o \to 0, \xi \to 0. \tag{41}$$

The asymptotic solutions (39) and (41) are identical, which explains an essentially vanishing error for e_2 in Fig. 2 as $\mathcal{W}_o \to 0$, and low values of e_2 overall in this low $\mathcal{W}_o$ number regime. Furthermore, the asymptotic solutions are linear in ξ, conforming to the boundary conditions at the wall at $\xi = 0$ and decaying to zero at the centerline given by $\xi = \mathcal{W}_o$, which is reflected in the corresponding velocity plots in Figs. 3(a) and 3(b).

As far as the solution of the standard Stokes' second problem is concerned, its asymptotic expansion is different. The most significant difference is the absence of $\mathcal{W}_o$ in the expansion, which prevents the solution from dropping to zero at $\xi = \mathcal{W}_o$, and, in fact, accounts for an essentially flat profile independent of ξ for small ξ, which can be observed from Figs. 3(a) and 3(b).

Linear behavior of solutions at small Womersley number can also be explained from a physical point of view. For a cylindrical domain, for such a small radius, the velocity profile at each time instance corresponds to that of a pure solid-body rotation with $u_\theta \propto r$. Likewise, the finite domain Cartesian solution behaves like a planar Couette flow at any given phase. This situation corresponds to almost an instantaneous adjustment of the flow to any given wall velocity.

Physically this occurs when the viscous timescale is much shorter than the oscillation period, given by the following relation:

$$\frac{\delta^2}{\nu} \ll T_{osc} \to \omega\left(\frac{\delta^2}{\nu}\right) \ll 2\pi \to \mathcal{W}_o \ll \sqrt{2\pi}. \tag{42}$$

This represents the state of the flow when the momentum transfer from the wall happens much faster than the oscillation period completes. This can occur when either the domain is small, the viscosity is large, or the oscillation period is large.

2. Intermediate Womersley number flow: Region of maximum e_2 error

In this section, we consider a regime of intermediate Womersley numbers $0.1 \lesssim \mathcal{W}_o \lesssim \mathcal{W}_o^{SI}$, where e_2 error exhibits its maximum at $\mathcal{W}_o \approx 3.26$. This Womersley number is sufficiently large that the asymptotic expansions developed in Sec. II are no longer valid, and sufficiently small that the expansions developed in Sec. IV for very large Womersely numbers are not valid as well.

The velocity profiles for the three considered Stokes' problems at $\mathcal{W}_o = 3.26$ are presented in Figs. 4(a) and 4(b). While the classical Stokes' second problem solution (HOW) deviates from both OPW and APW, the two finite domain solutions (cylindrical – OPW and Cartesian – APW) are no longer in perfect agreement, despite the match of the boundary conditions, due to the curvature effects. Since the domain thickness does not contribute to the error between the

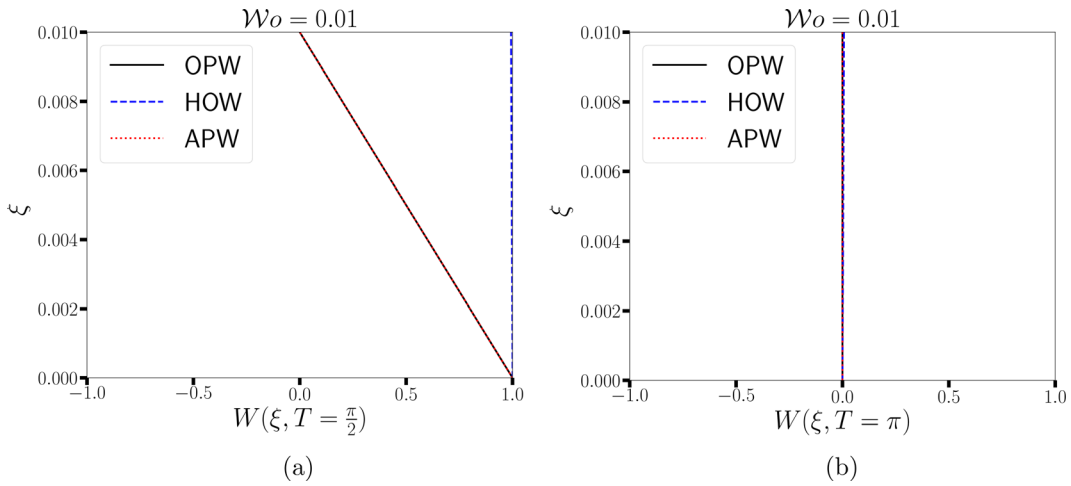

FIG. 3. (a) and (b) Velocity profiles at two selected phases at a low Womersley number $\mathcal{W}_o = 0.01$. Black solid line, cylindrical solution (OPW); blue dashed line, standard Stokes' second problem solution (HOW); red dotted line, finite domain Cartesian solution (APW). Black solid line and red dotted line lie on top of each other. Note at maximum wall velocity the HOW solution is a near vertical line for $\xi \in [0, \mathcal{W}_o]$ in (a).

APW and OPW solutions whose domain sizes (wall to wall cross-sectional distances) match, the curvature effects are clearly maximized at this Womersley number.

3. High Womersley number flow

Finally, we consider the region of a high Womersley number flow, $\mathcal{W}_o \gtrsim \mathcal{W}_o^{Sl}$. The significance of $\mathcal{W}_o^{Sl}$ defined in Eq. (34) is that above this Womersley number, the finite domain effects should be diminished, since for this layer thickness, the Stokes' layer velocity has decayed sufficiently, so that the finite and infinite domain problems might be a good approximation of each other.

To understand the behavior of solutions at high $\mathcal{W}_o$ regime, we, again, consider, an asymptotic expansion of the corresponding solutions, but at $\mathcal{W}_o \to \infty$.

HOW. The HOW solution given by Eq. (25) does not contain $\mathcal{W}_o$, so it is already in the form amenable to analysis at $\mathcal{W}_o \to \infty$, i.e., we can conclude that

$$W_1(\xi, T) \sim \Im\left\{ \exp(iT) \exp\left(-\sqrt{i}\xi\right)\right\}, \quad \mathcal{W}_o \to \infty. \tag{43}$$

APW. Using the approximation $\sinh^{-1}\left(\sqrt{i}\mathcal{W}_o\right) \sim 2\exp\left(-\sqrt{i}\mathcal{W}_o\right), \mathcal{W}_o \to \infty$, one can show that an anti-phase parallel walls solution given by Eq. (27) has an asymptotic expansion

$$W_2(\xi, T) \sim \Im\left\{ \exp(iT) \exp\left(-\sqrt{i}\xi\right)\right\}, \quad \mathcal{W}_o \to \infty, \tag{44}$$

which coincides with the standard Stokes' second problem solution asymptotics given by Eq. (43).

OPW. To consider the cylindrical (OPW) solution as $\mathcal{W}_o \to \infty$, we note that, for large values of z, an asymptotic form of the Bessel function exists as

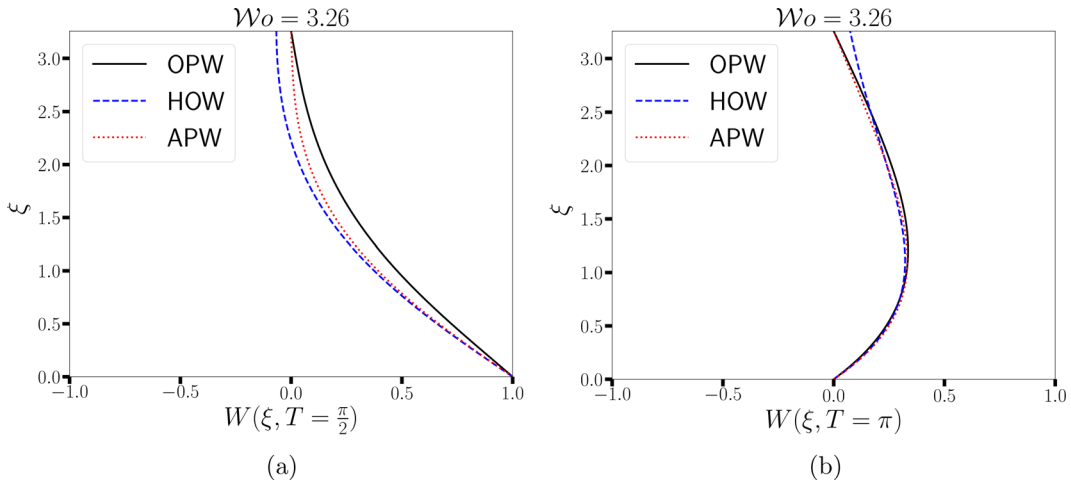

FIG. 4. Velocity profiles at two selected phases, (a) $T = \frac{\pi}{2}$ and (b) $T = \pi$, at a region of maximum e_2 error $\mathcal{W}_o = 3.26$. Black solid line, cylindrical solution (OPW); blue dashed line, standard Stokes' second problem solution (HOW); red dotted line, finite domain Cartesian solution (APW).

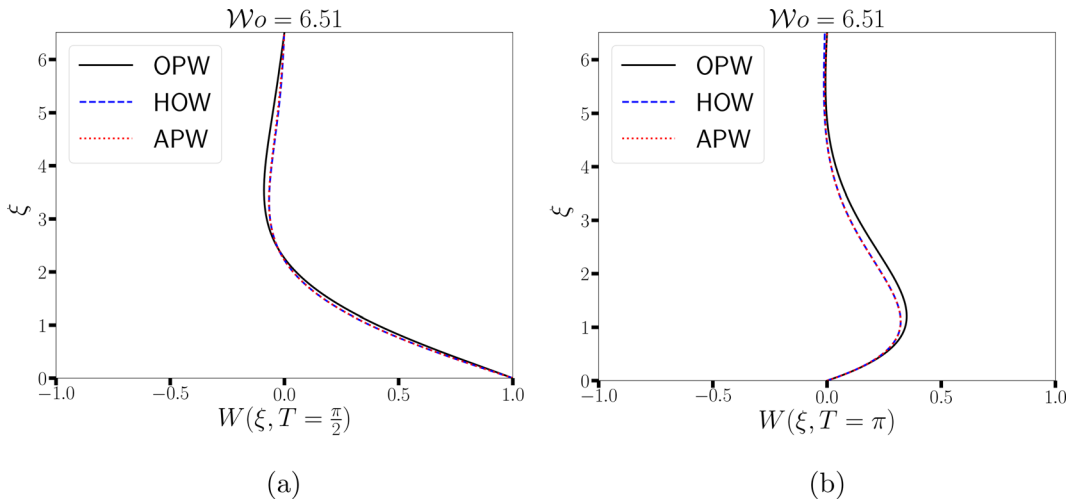

FIG. 5. (a) and (b) Velocity profiles at two selected phases at $\mathcal{W}_o = \mathcal{W}_o^{Sl} = 6.51$. Black solid line, cylindrical solution (OPW); blue dashed line, standard Stokes' second problem solution (HOW); red dotted line, finite domain Cartesian solution (APW).

$$J_1(z) \sim \sqrt{\frac{2}{\pi z}} \cos\left(z - \frac{3\pi}{4}\right), \quad |z| \gg \frac{3}{4}. \tag{45}$$

With some trigonometric manipulation, Eq. (45) can be rewritten as

$$J_1(z) \sim \sqrt{\frac{2}{\pi z}} \left(-i \sinh\left(i\left(z - \frac{\pi}{4}\right)\right)\right), \quad |z| \gg \frac{3}{4}, \tag{46}$$

or, alternatively,

$$J_1^{-1}\left(\sqrt{i^3}\mathcal{W}_o\right) \sim \sqrt{\frac{\pi z}{2}} 2\, i \sqrt{\mathcal{W}_o} \exp\left(-\sqrt{i}\mathcal{W}_o - \frac{\pi}{4} i\right), \quad \mathcal{W}_o \gg \frac{3}{4}, \tag{47}$$

from where we can write the asymptotic expression

$$W_{\text{cyl}}(\xi, T) \sim \Im\left\{ \exp(iT)\left(1 + \frac{1}{2}\frac{\xi}{\mathcal{W}_o}\right) \exp\left(-\sqrt{i}\xi\right)\right\}, \quad \mathcal{W}_o \to \infty. \tag{48}$$

While it is seen that an asymptotic decay of a cylindrical solution (OPW) as $\mathcal{W}_o \to \infty$ is the same as of the two Cartesian solutions (HOW and APW), the decay is slower at high but not infinite Womersley numbers due to a multiplication by $(1 + \xi/(2\mathcal{W}_o)) > 1$.

These effects are illustrated in Figs. 5 and 6, where the velocity profiles are plotted for $\mathcal{W}_o^{Sl} = 6.51$ and a relatively high $\mathcal{W}_o = 45.12$. It is seen that at a Womersley number based on the Stokes' layer thickness, both Cartesian solutions are aligned, as expected, while a cylindrical solution deviates from it slightly due to a different asymptotic behavior at this high-intermediate regime (see Fig. 5). However, for

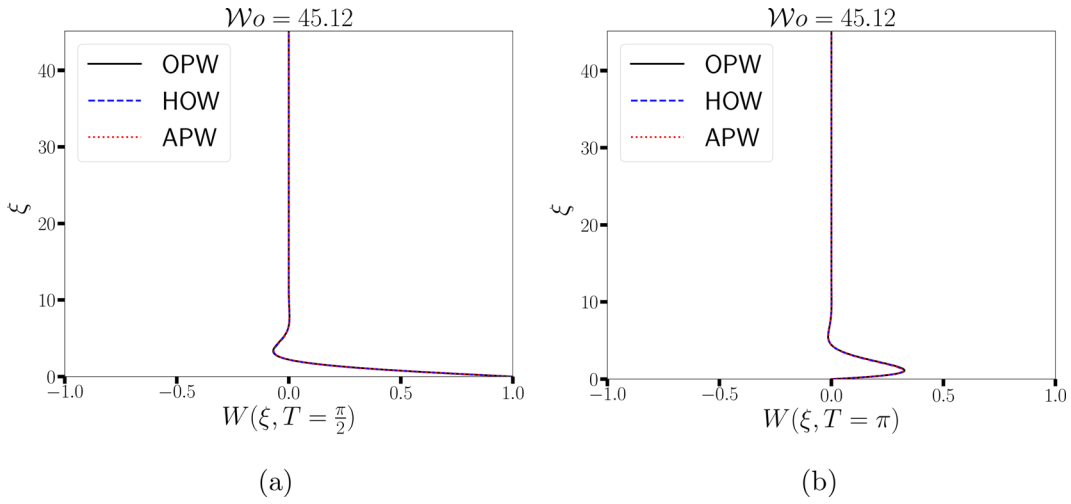

FIG. 6. (a) and (b) Velocity profiles at two selected phases at a high Womersley number $\mathcal{W}_o = 45.12$. Black solid line, cylindrical solution (OPW); blue dashed line, standard Stokes' second problem solution (HOW); red dotted line, finite domain Cartesian solution (APW).

$\mathcal{W}_o = 45.12$ in Fig. 6, all three velocity profiles are in perfect agreement. Likewise, errors e_1 and e_2 in the regime $\mathcal{W}_o \gtrsim \mathcal{W}_o^{Sl}$ are similar, since the profiles $W_1(\xi, T)$ and $W_2(\xi, T)$ essentially coincide. Both errors are getting smaller with the increase in Womersley number, since the cylindrical solution gets closer and closer to the two Cartesian solutions.

E. Discussion of the effects of curvature vs domain thickness

Two distinct effects contribute to the difference between the cylindrical Stokes' second problem solution (OPW) and the standard Stokes' second problem solution (HOW): the effect of curvature and the effect of the domain thickness. To help separate the influence of these effects, a comparison of a cylindrical solution (OPW) to a finite size Cartesian domain solution (APW) was considered, because it eliminates the domain thickness effects and only leaves the curvature effects. From this comparison (manifested in the error e_2), it is seen that the errors due to curvature are very small at low $\mathcal{W}_o$ numbers, where the viscous effects are dominant, they increase reaching the maximum around $\mathcal{W}_o \approx 3.26$ and then decrease at high $\mathcal{W}_o$ numbers due to an effective reduction in curvature. Finite domain effects, observable in the e_1 error between the cylindrical (OPW) solution and the standard Stokes' (HOW) solution, are the largest at low $\mathcal{W}_o$, where the different near-wall behavior of the two solutions constitutes the major component of the e_1 error and then monotonically decrease. In the regime of $0 < \mathcal{W}_o \lesssim 3.26$, while the error due to finite domain decreases, the error due to curvature increases, resulting in a low decrease rate of the overall e_1 error (between OPW and HOW) with $\mathcal{W}_o$. When $\mathcal{W}_o$ reaches $\mathcal{W}_o^{Sl} = 4.6\sqrt{2} \approx 6.51$, the finite domain error is sufficiently small and can be neglected, while the curvature error decreases, resulting in a collapse of the e_1 and e_2 errors, and a faster rate of decrease in both errors compared to the decrease in e_1 error in a low to intermediate $\mathcal{W}_o$ regime. Finally, since the e_1 error contains a combined contribution from both the finite domain error and the curvature error, the difference between the cylindrical (OPW) and the standard Stokes' (HOW) solution is always larger than the difference between cylindrical (OPW) and a finite size domain Cartesian (APW) solution.

IV. REMARKS ON APPLICATION TO TURBULENT DRAG REDUCTION

We are now interested to see how the above-mentioned findings regarding the difference in velocity profiles between the Stokes' problem solutions effect the conclusions that can be made during investigation of turbulent drag reduction in pipe and channel flows. In a turbulent regime, the flow is typically characterized by its friction Reynolds number,

$$Re_\tau = (u_\tau \delta_h)/\nu, \tag{49}$$

where u_τ is the friction velocity, and δ_h equals to h or $D/2$ is the outer length scale of the flow.[30] We now define the inner length and time scales $\delta_\tau = \nu/u_\tau, t_\tau = \nu/u_\tau^2$, which lead to the definition of the wall units as

$$y^+ = \frac{y}{\delta_\tau}, \quad T^+ = \frac{T}{t_\tau}. \tag{50}$$

From these definitions, we can scale the spanwise velocity profile in terms of the streamwise turbulent scalings. Namely, we can show that Stokes' thickness α expressed in terms of wall units is

$$\alpha = \sqrt{\frac{\nu}{\omega}} = \frac{\nu}{u_\tau}\sqrt{\frac{1}{2\pi f^+}}, \tag{51}$$

where $f^+ = \omega t_\tau/(2\pi)$ is the non-dimensional frequency of wall oscillations expressed in wall units. We can then write the Womersley number defined in Eq. (14) in terms of the wall units as

$$\mathcal{W}_o = Re_\tau\sqrt{2\pi f^+}. \tag{52}$$

At $\mathcal{W}_o \approx \mathcal{W}_o^{Sl} = 6.51$, the L_2 error value normalized by the wall velocity amplitude between the classical Stokes' second problem and the cylindrical solution is shown to be on the order of 10^{-3} in Fig. 2, and even smaller if the infinite and finite domain Cartesian solutions are compared, which is deemed sufficient for the classical Stokes' second problem (HOW) to be a reasonable approximation to the Stokes' solution obtained either in a pipe (OPW) or a channel (APW) geometry. Applying a criterion $\mathcal{W}_o > \mathcal{W}_o^{Sl}$, we find that

$$Re_\tau\sqrt{2\pi f^+} > \mathcal{W}_o^{Sl}, \tag{53}$$

which can be rearranged as

$$Re_\tau > Re_\tau^{Sl}, \tag{54}$$

with

$$Re_\tau^{Sl} = \frac{\mathcal{W}_o^{Sl}}{\sqrt{2\pi f^+}}. \tag{55}$$

Substituting $\mathcal{W}_o^{Sl} = 4.6\sqrt{2}$ and $f^+ = 0.01$ as the experimentally and numerically measured optimum frequency of wall oscillation for turbulent drag reduction[4,31] into Eq. (54), we find that $Re_\tau^{Sl} = 25.95$, and the following criterion on the Reynolds number holds:

$$Re_\tau > 25.95, \tag{56}$$

for which the classical Stokes' second problem solution can be applied to a cylindrical or a finite domain Cartesian geometry with a relative error of less than 10^{-3} or 0.1%. Since the flow in a pipe or a channel only becomes turbulent when $Re_\tau \gtrsim 150$, see, for example, Ref. 30, for the regime, where the turbulent drag reduction is of interest, the criterion (56) is naturally satisfied for all turbulent flows with $f^+ = 0.01$. This justifies an application of a standard Stokes' second problem solution to the phase-averaged azimuthal velocity profiles with a spanwise wall oscillation with traditional, relatively high, frequencies ($f^+ \sim 0.01$) proposed for drag reduction,[4,25,31] in a turbulent pipe or channel flow without incurring significant errors.

However, Marusic *et al.*[32] showed that drag reduction could be achieved more efficiently by modifying the frequency of oscillation to modulate large scales of motion in the outer layer. With this new idea, the frequencies of oscillation as low as $f^+ = 10^{-3}$ were successfully tried. For these low frequencies, the criterion of Eq. (56) would increase threefold, and, for even lower frequencies, it could happen that the Womersley number of the flow would become low enough that the classical Stokes' layer solution would no longer fall within the regime of validity for a solution comparison between the finite and

infinite domains, and researchers need to be cautioned of this possibility.

Another word of caution is that a laminar solution to the Stokes' second problem can only be applied to drag reduction studies, when the Stokes' layer stays laminar. A laminar-to-turbulent transition of the Stokes' layer was measured to occur at a Reynolds number of $Re_\delta^{Sp} = (w_o\delta^{Sp})/\nu \gtrsim 550$ based on the wall oscillation amplitude and the Stokes' penetration depth.[27,33,34] Given the relationship (33) between the Stokes' penetration depth and the Stokes' layer thickness, we can rewrite this criterion in terms of the Stokes' layer thickness conventionally used in this paper: $Re_\delta^{Sl} = (w_o\delta^{Sl})/\nu \gtrsim 2530$. It can be shown that $Re_{\delta^{Sl}}$ can be expressed as

$$Re_\delta^{Sl} = w_0^+ Re_\tau^{Sl}, \tag{57}$$

with Re_τ^{Sl} as defined above in Eq. (55). Given that $\mathcal{W}_o^{Sl}$ is precisely defined by (34), and the critical Re_δ^{Sl} come from the measurements,[27,33] we can write the following criterion for the laminar-to-turbulent transition in an oscillatory Stokes' layer:

$$\frac{w_o^+}{\sqrt{f^+}} \gtrsim \frac{\sqrt{2\pi}\cdot 2530}{\mathcal{W}_o^{Sl}} \approx 975. \tag{58}$$

Using $f^+ = 0.01$ as before, and $w_o^+ = 10$ as the wall oscillation amplitude located within an optimum range for drag reduction as reported in the previous studies,[4,31] we can see that $w_o^+/\sqrt{f^+} \approx 100$ in a wall oscillation regime with relatively high frequencies, so that the criterion (58) is satisfied, and the Stokes' layer stays laminar.[24,25,31] However, with low frequencies,[32] and depending on the wall oscillation amplitude, the ratio $w_o^+/\sqrt{f^+}$ could fall in the range of the criterion of (58), the Stokes' layer would become turbulent and completely different solution properties in the Stokes' layer could be achieved.

V. CONCLUSION

We have considered three laminar solutions to the Stokes' second problem. We have shown that a single non-dimensional parameter, the Womersley number, completely defines the problem with respect to the domain size and the wall oscillation frequency. We have demonstrated an existence of three distinct regimes of Womersley numbers as related to the differences between the cylindrical (OPW) and Cartesian (HOW, APW) Stokes' problem solutions. (1) A small Womersley number regime characterized by $\mathcal{W}_o \lesssim 0.1$, where the two finite-domain solutions are asymptotically equivalent, and the infinite-domain standard Stokes' solution deviates significantly due to the finite-domain effects. The fact that cylindrical and flat-plate solutions are equivalent in this regime can be physically explained by the existence of a linear velocity profile in both cases established due to a diminutive ratio of the viscous timescale to the oscillation period occurring when $\mathcal{W}_o \ll \sqrt{2\pi}$. In this regime, the curvature errors are small, and the finite-domain errors are large. (2) A large Womersley number regime defined as $\mathcal{W}_o \gtrsim \mathcal{W}_o^{Sl} = 4.6\sqrt{2}$, where two Cartesian solutions are asymptotically equivalent, and the cylindrical solution deviates slightly, with the difference being small and rapidly decreasing with $\mathcal{W}_o$. In this regime, the finite-domain error is negligible, while the curvature error exists but is small and further drops with $\mathcal{W}_o$. (3) In the intermediate $\mathcal{W}_o$ regime, both errors are significant, and all three solutions deviate from each other.

Based on the error analysis, we show that for a classical Stokes' second problem solution to serve as a good approximation for an oscillating Stokes' layer in a pipe or a channel, the Womersley number of the flow in a pipe or a channel must be greater than the Womersley number based on the Stokes' layer thickness $\mathcal{W}_o > \mathcal{W}_o^{Sl} = 4.6\sqrt{2}$. In fact, in this regime, the L_2 error between the cylindrical and the classical Stokes' solution is guaranteed to be less than 0.1% of the wall oscillation amplitude, and even smaller when the classical and the finite-width Cartesian solutions are compared. When the Womersley criterion is recast in terms of wall units relevant in the studies of turbulent drag reduction with a spanwise-oscillating wall, and the non-dimensional frequency of $f^+ = 0.01$ is used as a typical oscillation frequency in turbulent drag reduction studies,[25,31] we obtain a criteria that $Re_\tau > 25.95$ for the L_2 error between all three solutions to fall below 0.1%. Since the longitudinal boundary layer flow is turbulent only at $Re_\tau \gtrsim 150$, the current work confirms that the application of a classical Stokes' layer solution to study turbulent drag reduction in pipes and channels at these, relatively high, oscillation frequencies, is appropriate. Furthermore, using the information from the previous experimental and computational work,[27,33–35] we show that in the regime of interest to turbulent drag reduction with the spanwise wall oscillation at $f^+ = 0.01$, the Stokes' layer remains laminar. At lower wall oscillation frequencies,[32] both the similarity criterion between the Stokes' solutions and the laminar-to-turbulent transition criterion of the Stokes' layer need to be reevaluated, as lower oscillation frequencies effectively lower the Womersley number of the flow, conducive both to larger solution differences, and to earlier transitions in the Stokes' layer. The application of wall oscillations can be employed to reduce drag in pipelines, which would lower the cost of pumping and lead to energy savings.

ACKNOWLEDGMENTS

This research was supported by the Ira A. Fulton Endowment and by the NSF CAREER Award No. CBET-1944568.

AUTHOR DECLARATIONS

Conflict of Interest

The authors have no conflicts to disclose.

Author Contributions

Daniel Coxe: Data curation (lead); Formal analysis (equal); Writing – original draft (lead); Writing – review & editing (equal). **Yulia T. Peet:** Formal analysis (equal); Writing – review & editing (equal). **Ronald J. Adrian:** Formal analysis (equal); Writing – review & editing (equal).

DATA AVAILABILITY

The data that support the findings of this study are available from the corresponding author upon reasonable request.

APPENDIX A: DERIVATION OF THE ANTI-PHASE PARALLEL WALL SOLUTION

Here, we derive a solution to a modified Stokes' second problem in a finite-height domain bounded by the infinitely long plates

located at $y = -h$ and $y = h$, whose solution did not yet appear in the literature. As stated in Sec. II B, in its non-dimensional form, this problem is governed by Eq. (4) with boundary conditions (12) and (13).

We are looking for a fully developed periodic in time solution and thus neglect initial transients. A separation of variables technique applied to this situation yields

$$W(Y,T) = \Im\{\exp(iT)F(Y)\}. \tag{A1}$$

Substituting the form of the solution given by Eq. (A1) to the governing equation (4) we obtain the following differential equation:

$$iF(Y) - \frac{d^2F(Y)}{dY^2} = 0. \tag{A2}$$

This equation has a complex exponential solution given by

$$F(Y) = c_1 \exp\left(\sqrt{i}Y\right) + c_2 \exp\left(-\sqrt{i}Y\right). \tag{A3}$$

From the boundary conditions, we obtain a set of linear equations for c_1 and c_2,

$$c_1 \exp\left(-\sqrt{i}\mathcal{W}_o\right) + c_2 \exp\left(\sqrt{i}\mathcal{W}_o\right) = 1, \tag{A4}$$

$$c_1 \exp\left(\sqrt{i}\mathcal{W}_o\right) + c_2 \exp\left(-\sqrt{i}\mathcal{W}_o\right) = -1. \tag{A5}$$

Solving for c_1, c_2 from (A4) and (A5), we arrive at the form of the solution given by

$$W(Y,T) = \Im\left\{-\exp(iT)\frac{\sinh\left(\sqrt{i}Y\right)}{\sinh\left(\sqrt{i}\mathcal{W}_o\right)}\right\}. \tag{A6}$$

APPENDIX B: DERIVATION OF A TIME-PERIODIC SOLUTION TO OSCILLATING PIPE WALL PROBLEM

In cylindrical coordinates, the equations of motion for the Stokes' second problem reduce to

$$\frac{\partial W}{\partial T} - \left(\frac{1}{R}\frac{\partial}{\partial R}\left(R\frac{\partial W}{\partial R}\right) - \frac{W}{R^2}\right) = 0. \tag{B1}$$

Boundary conditions are specified as

$$W(R = \mathcal{W}_o, T) = \sin(T), \tag{B2}$$

$$W(R = 0, T) = 0. \tag{B3}$$

In Eqs. (B1)–(B3), the variables are made dimensionless using the relations (20)–(24)

For a fully developed time-periodic solution, we seek its representation using a separation of variables technique

$$W(R,T) = \Im\{\exp(iT)F(R)\}. \tag{B4}$$

With the form of the solution given by (B4), the governing equation (B1) together with the boundary conditions (B2) and (B3) yields the following boundary value problem:

$$iF(R) - \left(\frac{d^2F(R)}{dR^2} + \frac{1}{R}\frac{dF(R)}{dR} - \frac{1}{R^2}F(R)\right) = 0, \tag{B5}$$

$$F(0) = 0, \tag{B6}$$

$$F(\mathcal{W}_0) = 1. \tag{B7}$$

Re-arranging equation (B5), one gets

$$R^2\frac{d^2F(R)}{dR^2} + R\frac{dF(R)}{dR} - (iR^2 + 1)F(R) = 0. \tag{B8}$$

Recognizing that Eq. (B8) is in the form of the modified Bessel equation, one can immediately write a solution to it as[29]

$$F(R) = c_1 I_1(i^{1/2}R) + c_2 K_1(i^{1/2}R). \tag{B9}$$

Here, I_1 and K_1 are the modified Bessel functions of the first and second kind, respectively. Noting that we require the rotation rate to be finite at the center, we can set c_2 to be zero. For a more conventional representation, we further transform the solution to be written in terms of standard Bessel functions as opposed to the modified ones. This can be done using the relation

$$I_n(z) = i^{-n}J_n(iz), \tag{B10}$$

where J_n is the Bessel function of the first kind. Applying this to Eq. (B9) gives a full solution of the following form:

$$W(R,T) = c'\exp(iT)J_1\left(\sqrt{i^3}R\right), \tag{B11}$$

which, after applying the boundary condition at the wall, gives

$$W(R,T) = \Im\left\{\exp(iT)\frac{J_1\left(\sqrt{i^3}R\right)}{J_1\left(\sqrt{i^3}\mathcal{W}_o\right)}\right\}. \tag{B12}$$

REFERENCES

[1] H. Choi, P. Moin, and J. Kim, "Active turbulence control for drag reduction in wall-bounded flows," J. Fluid Mech. **262**, 75–110 (1994).
[2] J. Yao, X. Chen, and F. Hussain, "Reynolds number effect on drag control via spanwise wall oscillation in turbulent channel flows," Phys. Fluids **31**, 085108 (2019).
[3] K.-S. Choi and M. Graham, "Drag reduction of turbulent pipe flows by circular-wall oscillation," Phys. Fluids **10**, 7–9 (1998).
[4] M. Quadrio and P. Ricco, "Critical assessment of turbulent drag reduction through spanwise wall oscillations," J. Fluid Mech. **521**, 251–271 (2004).
[5] R. L. Panton, *Incompressible Flow* (John Wiley & Sons, 2013).
[6] C.-M. Liu and I.-C. Liu, "A note on the transient solution of Stokes' second problem with arbitrary initial phase," J. Mech. **22**, 349–354 (2006).
[7] F. Laadhari, L. Skandaji, and R. Morel, "Turbulence reduction in a boundary layer by a local spanwise oscillating surface," Phys. Fluids **6**, 3218–3220 (1994).
[8] D. Zhou and K. S. Ball, "Turbulent drag reduction by spanwise wall oscillations," Int. J. Eng. **21**, 85–104 (2008).
[9] E. Touber and M. A. Leschziner, "Near-wall streak modification by spanwise oscillatory wall motion and drag-reduction mechanisms," J. Fluid Mech. **693**, 150–200 (2012).
[10] P. Ricco and M. Quadrio, "Wall-oscillation conditions for drag reduction in turbulent channel flow," Int. J. Heat Fluid Flow **29**, 891–902 (2008).
[11] Y. Song and M. J. Rau, "Viscous fluid flow inside an oscillating cylinder and its extension to Stokes' second problem," Phys. Fluids **32**, 043601 (2020).
[12] P. Ricco, M. Skote, and M. A. Leschziner, "A review of turbulent skin-friction drag reduction by near-wall transverse forcing," Prog. Aerosp. Sci. **123**, 100713 (2021).
[13] A. Yakeno, "Drag reduction and transient growth of a streak in a spanwise wall-oscillatory turbulent channel flow," Phys. Fluids **33**, 065122 (2021).
[14] J. Sherwood, "Unsteady flow adjacent to an oscillating or impulsively started porous wall," J. Fluid Mech. **894**, A1 (2020).

[15]Y.-M. Chu, S. Bashir, M. Ramzan, and M. Y. Malik, "Model-based comparative study of magnetohydrodynamics unsteady hybrid nanofluid flow between two infinite parallel plates with particle shape effects," Math. Methods Appl. Sci. 1–15 (2022).
[16]M. Ramzan, N. Shahmir, H. A. S. Ghazwani, and M. Malik, "Comparative appraisal of nanofluid flows in a vertical channel with constant wall temperatures: An application to the rocket engine nozzle," in *Waves in Random and Complex Media* (2022), pp. 1–24.
[17]M. Ramzan, S. Riasat, S. F. Aljurbua, H. A. S. Ghazwani, and O. Mahmoud, "Hybrid nanofluid flow induced by an oscillating disk considering surface catalyzed reaction and nanoparticles shape factor," Nanomaterials **12**, 1794 (2022).
[18]S. Riasat, M. Ramzan, Y.-L. Sun, M. Malik, and R. Chinram, "Comparative analysis of Yamada-Ota and Xue models for hybrid nanofluid flow amid two concentric spinning disks with variable thermophysical characteristics," Case Stud. Therm. Eng. **26**, 101039 (2021).
[19]M. Uddin and A. Murad, "Stokes' second problem and oscillatory Couette flow for a two-layer fluid: Analytical solutions," Alexandria Eng. J. **61**, 10197–10218 (2022).
[20]C. H. Hor, C. P. Tso, G. M. Chen, and C. K. Kok, "Characteristics of the internal fluid flow field induced by an oscillating plate with the other parallel plate stationary," J. Adv. Res. Fluid Mech. Therm. Sci. **55**, 136–141 (2019).
[21]C.-M. Liu, "Complete solutions to extended Stokes' problems," Math. Problems Eng. **2008**, 754262.
[22]G. Riccardi, "Remarks on the solution of extended Stokes' problems," Int. J. Non-Linear Mech. **46**, 958–970 (2011).
[23]Y. Zeng and S. Weinbaum, "Stokes problems for moving half-planes," J. Fluid Mech. **287**, 59–74 (1995).
[24]M. Quadrio and S. Sibilla, "Numerical simulation of turbulent flow in a pipe oscillating around its axis," J. Fluid Mech. **424**, 217–241 (2000).
[25]D. J. Coxe, Y. T. Peet, and R. J. Adrian, "Vorticity statistics and distributions in drag reduced turbulent pipe flow with transverse wall oscillations," in Proceedings of 11th International Symposium on Turbulence and Shear Flow Phenomena, Southampton, UK, 2019.
[26]N. Bruot, P. Cicuta, H. Bloomfield-Gadêlha, R. E. Goldstein, J. Kotar, E. Lauga, and F. Nadal, "Direct measurement of unsteady microscale Stokes flow using optically driven microspheres," Phys. Rev. Fluids **6**, 053102 (2021).
[27]R. Akhavan, R. Kamm, and A. Shapiro, "An investigation of transition to turbulence in bounded oscillatory Stokes flows Part 1. Experiments," J. Fluid Mech. **225**, 395–422 (1991).
[28]C. Canuto, M. Y. Hussaini, A. Quarteroni, and T. A. Zang, *Spectral Methods in Fluid Dynamics* (Springer-Verlag, 1988).
[29]M. Abramowitz and I. A. Stegun, *Handbook of Mathematical Functions with Formulas, Graphs, and Mathematical Tables* (US Government Printing Office, 1970), Vol. 55.
[30]H. Schlichting and K. Gersten, *Boundary-Layer Theory* (Springer, 2016).
[31]J.-I. Choi, C.-X. Xu, and H. J. Sung, "Drag reduction by spanwise wall oscillation in wall-bounded turbulent flows," AIAA J. **40**, 842–850 (2002).
[32]I. Marusic, D. Chandran, A. Rouhi, M. K. Fu, D. Wine, B. Holloway, D. Chung, and A. J. Smits, "An energy-efficient pathway to turbulent drag reduction," Nat. Commun. **12**, 5805 (2021).
[33]T. Sarpkaya, "Coherent structures in oscillatory boundary layers," J. Fluid Mech. **253**, 105–140 (1993).
[34]G. Vittori and R. Verzicco, "Direct simulation of transition in an oscillatory boundary layer," J. Fluid Mech. **371**, 207–232 (1998).
[35]P. Costamagna, G. Vittori, and P. Blondeaux, "Coherent structures in oscillatory boundary layers," J. Fluid Mech. **474**, 1–33 (2003).